Renewable Energy 161 (2020) 133–148

Contents lists available at ScienceDirect

Renewable Energy

journal homepage: www.elsevier.com/locate/renene

Understanding the behaviour of naturally-ventilated BIPV modules: A sensitivity analysis

Juliana E. Gonçalves [a, b, *], Twan van Hooff [a, c], Dirk Saelens [a, b]

[a] Building Physics Section, Department of Civil Engineering, KU Leuven, Kasteelpark Arenberg 40, 3001, Leuven, Belgium
[b] EnergyVille I, Thor Park 8310, 3600, Genk, Belgium
[c] Building Physics and Services Unit, Department of the Built Environment, Eindhoven University of Technology (TU/e), P.O. Box 513, 5600 MB, Eindhoven, the Netherlands

ARTICLE INFO

Article history:
Received 29 January 2020
Received in revised form
3 June 2020
Accepted 18 June 2020
Available online 25 July 2020

Keywords:
Building integrated photovoltaic (BIPV)
Sensitivity analysis
Natural ventilation
Exterior convective heat transfer coefficient
Building facades
Solar energy

ABSTRACT

Building integrated photovoltaic (BIPV) is a key concept for the realisation of sustainable buildings. Despite the progress in BIPV modelling, the use of sensitivity analysis (SA) is still scarce in the BIPV literature. SA can help the modeller to identify which model inputs influence the model outputs the most. This paper presents a simulation framework that combines global SA methods with a multi-physics BIPV model. The analysis focuses on the performance of naturally ventilated BIPV facade elements (cell temperature and power). Building performance indicators, such as the total heat flux to the building interior and the building wall temperature, are also analysed. Inputs to the SA include convective heat transfer coefficients, cavity airflow rate, and weather conditions. As expected, the SA results were found to be highly dependent on the range selected for the inputs. For a narrow variation in weather conditions, the exterior convective heat transfer coefficient was identified as the input with the strongest influence on the BIPV performance. Results also showed that cavity ventilation becomes more important as the exterior convective heat transfer decreases. These findings indicate the need for accurate models to represent exterior convective heat transfer in BIPV facades and corroborate the importance of cavity ventilation.

1. Introduction

In 2018, the building and construction sector accounted for 36% of global final energy use and 39% of energy and process-related carbon dioxide (CO_2) emissions [1]. By mid-century, the energy use in buildings and its related emissions are expected to double or even triple [2]. To mitigate the impact on the energy system and the climate, governments all around the world have improved the existing building energy codes and/or proposed new regulations for the sector [3]. In general, the road-map towards sustainable buildings involves improvements in energy efficiency for new and existing buildings as well as the deployment of renewable energy sources (RES) in the built environment [2]. Well established technologies such as photovoltaic (PV) systems are key to increase the RES share in the built environment [2,4,5]. So far, the PV deployment in the built environment has been mostly limited to building applied photovoltaics (BAPV) applications, in which the PV modules are attached to the building envelope, normally on the roof. For aesthetic reasons, BAPV applications are not common on building facades.

Alternatively, PV cells/films can be integrated into building elements, such as windows or facade elements, eliminating the need for the extra support structure. This concept is known as building integrated photovoltaics (BIPV). Besides producing electricity, BIPV elements provide at least one envelope function, such as insulation, weather barrier, or sun shading [6]. BIPV elements designed as high-performance building components are an interesting option for building renovation, as they can also improve the energy performance of the building [7,8]. In terms of aesthetics, the integrated concept of BIPV has the potential to facilitate the assimilation of PV in building facades [6,7]. This possibility is important because facades hold a significant solar potential in the urban environment, complementing the surface area available on rooftops [9]. For example, it has been shown that the PV potential in roofs and facades can exceed the local non-baseload demand and contribute to

* Corresponding author. Building Physics Section, Department of Civil Engineering, KU Leuven, Kasteelpark Arenberg 40, 3001, Leuven, Belgium.
E-mail address: juliana.goncalves@kuleuven.be (J.E. Gonçalves).

https://doi.org/10.1016/j.renene.2020.06.086
0960-1481/

Abbreviations

BAPV	Building applied photovoltaic
BIPV	Building integrated photovoltaic
CFD	Computational fluid dynamics
c-Si	Crystalline Silicon cells
eFAST	Extended fast Fourier amplitude sensitivity testing
MPP	Maximum power point
OAT	One-at-a-time
PV	Photovoltaic
RES	Renewable energy source
SA	Sensitivity analysis

Nomenclature

$\Delta T_{air,in}$	Increase in air temperature at the cavity inlet due to local heat transfer, °C
h_{ext}	Exterior convective heat transfer coefficient, W/(m^{2}K)
h_{indoor}	Indoor convective heat transfer coefficient, W/(m^{2}K)
h_{PV}	Convective heat transfer coefficient inside the BIPV cavity (PV surface), W/(m^{2}K)
h_{wall}	Convective heat transfer coefficient inside the BIPV cavity (building wall surface), W/(m^{2}K)
HF_{indoor}	Heat flux into the building interior, W/m^2
I_{POA}	Plane-of-array solar irradiance, W/m^2
m_{flow}	Airflow rate through the BIPV cavity, kg/(sm)
N	number of samples
P_{BIPV}	BIPV power, W
P_{STC}	BIPV power at standard test conditions, W
R_{wall}	Building wall thermal resistance, (m^{2}K)/W
$T_{air,in}$	Inlet air temperature, °C
T_{amb}	Ambient temperature, °C
T_{BIPV}	BIPV temperature, °C
T_{ground}	Ground temperature, °C
T_{indoor}	Indoor temperature, °C
T_{sky}	Sky temperature, °C
$T_{wall,cav}$	Cavity wall temperature, °C
$T_{wall,\ indoor}$	Building wall indoor temperature, °C

50–75% of the total electricity demand [10]. Furthermore, facades provide a balanced power profile over the day and the year, which can help to mitigate the mismatch between demand and supply, as discussed in e.g. Refs. [10–12].

Existing BIPV applications have been recently reviewed in several publications, e.g. Refs. [13–16]. These reviews show that the design of BIPV elements commonly includes a ventilated cavity, primarily used to reduce the PV operating temperatures. High operating temperatures are a well known cause of reduced power generation in PV systems [17]. This power loss is generally expressed by temperature coefficients, which depend on PV technology. For example, with a temperature coefficient of about 0.42%/°C, commercial crystalline silicon (c-Si) cells present a reduction in power of about 8% for a temperature increase of 20 °C above the standard test condition (i.e. cell temperature of 25 °C at solar irradiance of 1000 W/m^2). High operating temperatures also accelerate degradation mechanisms, reducing the lifetime of the PV module [18,19].

The performance assessment of ventilated BIPV facades is a complex task. It depends on several factors, such as the ventilation conditions in the cavity, material properties, wind flow around the building, etc. Parametric analyses have been used to investigate the individual effect of certain factors on the BIPV performance. For example, the theoretical study in Ref. [20] shows that the PV temperature decreases by 12 °C, when the emissivity of the PV module increases from 0 to 1. The same publication has shown that increasing the cavity thickness from 1 to 8 cm results in a decrease in PV temperature of 6 °C for an airflow velocity of 0.5 m/s [20]. Another example is the theoretical study in Ref. [21], which shows that the albedo has a linear effect on the annual BIPV energy yield, with variations between −1.0 and 0.5%. These parametric analyses can be considered a type of local sensitivity analysis, also known as one-at-a-time (OAT) sensitivity. An OAT approach is valuable to gain some insights into the effect of a single parameter on the BIPV performance at a relatively low computational cost. However, this approach has several limitations: it explores only a reduced input space, it does not consider interactions between inputs, and it is not able to explain how much of the output variation is accounted by the input factors [22]. Moreover, a local SA does not provide information on the uncertainty of the model outputs [23].

To understand the behavior of complex systems, global SA methods are more appropriate [24]. Global SA reveals which model inputs have the strongest influence on its predictions and how these inputs interact with each other [22,23,25]. This information helps the modellers to prioritise their efforts by focusing on the most important inputs/parameters [24]. However, despite the clear importance of global SA, the BIPV literature is still scarce in this respect. The use of global SA in the BIPV literature is limited to the work in Ref. [26], which uses SA within a data-driven approach to identify the unknown parameters of a dynamic model for naturally ventilated PV components. The coefficients related to the airflow and heat transfer as well as the optical properties of the BIPV module have been identified as strong parameters. These findings are very relevant, but they are related to the experimental data used to derive the model and are thus not generally applicable.

Another limitation of the parametric analyses performed so far in the BIPV field is that they mostly focus on cavity ventilation and material properties. A factor that deserves more attention in BIPV studies is the exterior convective heat transfer. In numerical models, the exterior convective heat transfer is normally described by the exterior convective heat transfer coefficient (h_{ext}). Recent research has discussed the limitations and uncertainty of existing h_{ext} models for building surfaces, e.g. Refs. [27–30]. In particular, the work in Ref. [28] tested several h_{ext} models to estimate the energy performance of a isolated, well-insulated building. The results show deviations up to ± 30% in the yearly cooling energy demand and ± 14% in the hourly peak cooling energy demand (in relation to the average result). These existing h_{ext} models have been extensively used in BIPV assessment as well. However, the impact of h_{ext} variations on the predicted BIPV performance has not been investigated yet.

The literature review shows that previous research mainly used AOT approaches (which do not consider the interactions between inputs) and mostly focused on cavity ventilation and material properties. This paper proposes a simulation framework based on global SA methods to investigate the behaviour of naturally ventilated BIPV facades. The systematic approach in this work results in recommendations for BIPV modelling. Using this SA framework, this paper addresses the following research questions: Which model inputs are most influential with respect to the BIPV behaviour? In particular, how does the BIPV model respond to variations in the exterior convective heat transfer? And, finally, how can this analysis help BIPV modellers in the future? The novelty in this work lies on (1) the use of global SA methods (which consider

interactions between inputs), and (2) the analysis of the exterior convective heat transfer as a key parameter in BIPV models.

The simulation framework combines global SA methods available in SALib [31] with a multi-physics BIPV model developed previously by the authors [32,33]. These earlier publications by the authors focused on validating the model using experimental field data (i.e. under realistic operating conditions). The novelty in the present work is to use the validated model within a SA framework to understand how the model responds to variations in its inputs (considering interactions between inputs). The inputs to the SA include convective heat transfer coefficients and the airflow through the BIPV cavity. These inputs are selected because they can be modified to some extent by changing the BIPV design. For example, the airflow rate can be increased by enlarging the cavity openings. In view of the complex wind flow in the built environment, the exterior convective heat transfer coefficient is also included in this analysis. Irradiance and ambient temperature are considered as inputs as well. The BIPV performance is analysed in terms of power and operating temperature (model outputs). The building wall temperature and the heat flux into the building are taken as additional outputs.

Section 2 introduces the multi-physics BIPV model used for the SA. Next, Section 3 presents the methodology employed in the SA. Section 4 presents the results, which are subsequently discussed in Section 5. Last, Section 6 summarises and concludes the paper.

2. Multi-physics BIPV model

The multi-physics BIPV model used in this work was described by the authors in previous publications [32,33]. This section only provides information relevant for the SA presented in this paper. Detailed information can be found in Refs. [32,33].

2.1. Model description

The multi-physics BIPV model combines a high-resolution electrical model with physics-based thermal and airflow models, as schematically illustrated in Fig. 1. This figure also shows how the BIPV model is coupled to the building zone, as an exterior building wall. The BIPV model follows a control volume approach, in which each BIPV control volume correspond to a single PV cell. A detailed representation of one BIPV control volume is shown in Fig. 2, indicating the main variables and heat transfer fluxes.

Using Figs. 1 and 2 as reference, the multi-physics BIPV model can be explained as follows. The electrical model calculates the power output (P_{BIPV}) using a one-diode approach, while the thermal and airflow models determine the BIPV cell temperature (T_{BIPV}). The power output is introduced in the thermal modelling as a heat sink for each PV cell. In turn, the cell temperature is used in the electrical model to estimate the power output (temperature-power coupling). The airflow (m_{flow}) through the cavity connects the control volumes vertically (airflow-temperature coupling). The solver iterates the solution until a default tolerance of 0.0001 for the state variables is achieved. Later on, Section 3 will describe how the BIPV model is used within the SA framework.

2.2. Experimental validation

The multi-physics BIPV model was validated using experimental data from field tests performed at the Vliet test building, located in Leuven, Belgium (Fig. 3a). Experimental data from two distinct c-Si BIPV modules were used to validate the model: a well-ventilated BIPV module and a curtain wall BIPV module (Fig. 3b). Both BIPV modules are integrated into the southwest facade of the Vliet building and, therefore, operate under realistic conditions as part of the building. The validation results are reported in detail in two previous publications by the authors [32,33]. The validation was based on power and back-of-module temperature measurements (Fig. 3b and c). A good agreement was observed between the model predictions and the experimental data. The daily energy yield is predicted with an average error below 5% and the back-of-module temperature with an average absolute difference below 2 °C. Further detailed information about the BIPV modules, on-site measurements, experimental accuracy, etc., is provided in Refs. [32,33]. Note that these previous publications by the authors focused on describing and validating the model using experimental field data. The novelty in the present work is to use the validated model within a SA framework to understand in a systematic way how the model responds to variations in its inputs.

2.3. Relevant inputs

The characteristics of the BIPV module used in the present study correspond to the BIPV curtain wall module, which was used to validate the multi-physics BIPV model in Ref. [33]. The BIPV curtain wall design follows the current guidelines for building elements, which makes it a realistic configuration in terms of size and materials. The composition of the BIPV curtain wall module is similar to the scheme presented in Fig. 2: it includes a glass-glass PV module, a ventilated air cavity, and a building wall. Table 1 presents the material properties of the BIPV module used in the simulations. The BIPV module is composed of 60 c-Si cells, with a PV area of $1 \times 1.5\ m^2$, and was rated at 244 W under standard test conditions (STC). In this BIPV module, the building wall corresponds to a single layer of insulation material. With a relatively thick layer of insulating material, this BIPV module is a well insulated building component. The influence of the building thermal resistance is investigated later in Section 4.2.1.

3. Sensitivity analysis

Fig. 4a illustrates the work flow defined for the SA. First, the problem is defined and the objectives of the SA are identified. A clear understanding of the problem is very important, as it defines which inputs and outputs are relevant and which input distributions are appropriate (normal vs. uniform). Second, the input variation ranges are defined. This task requires a comprehensive literature survey to define appropriate ranges for the inputs. Third, the input vectors are generated using sampling techniques available in the open-source Python library SALib [31]. Four, the input vectors are used in the multi-physics BIPV model described in Section 2 to generate the output vectors, as illustrated in Fig. 4b. These simulations are performed in openIDEAS/Modelica [34]. Last, the sensitivity measures are evaluated based on different SA methods, again using SALib [31].

3.1. Problem definition

Here, it is important to understand that sensitivity analyses can be used with different objectives. To explain the implications of different objectives, the author in Ref. [22] takes as example the thermo-physical properties of the building envelope. These properties can be associated to a normal distribution if the objective is to compare the simulated performance of an existing building to its monitored behaviour. Normal distributions account for natural uncertainties, due to, for example, construction aspects, aging, and actual conditions of the building. In contrast, if the goal is to identify energy saving measures at the early design stage, these properties should be taken as equally probable and related to a uniform distribution, as the materials composing the walls have not

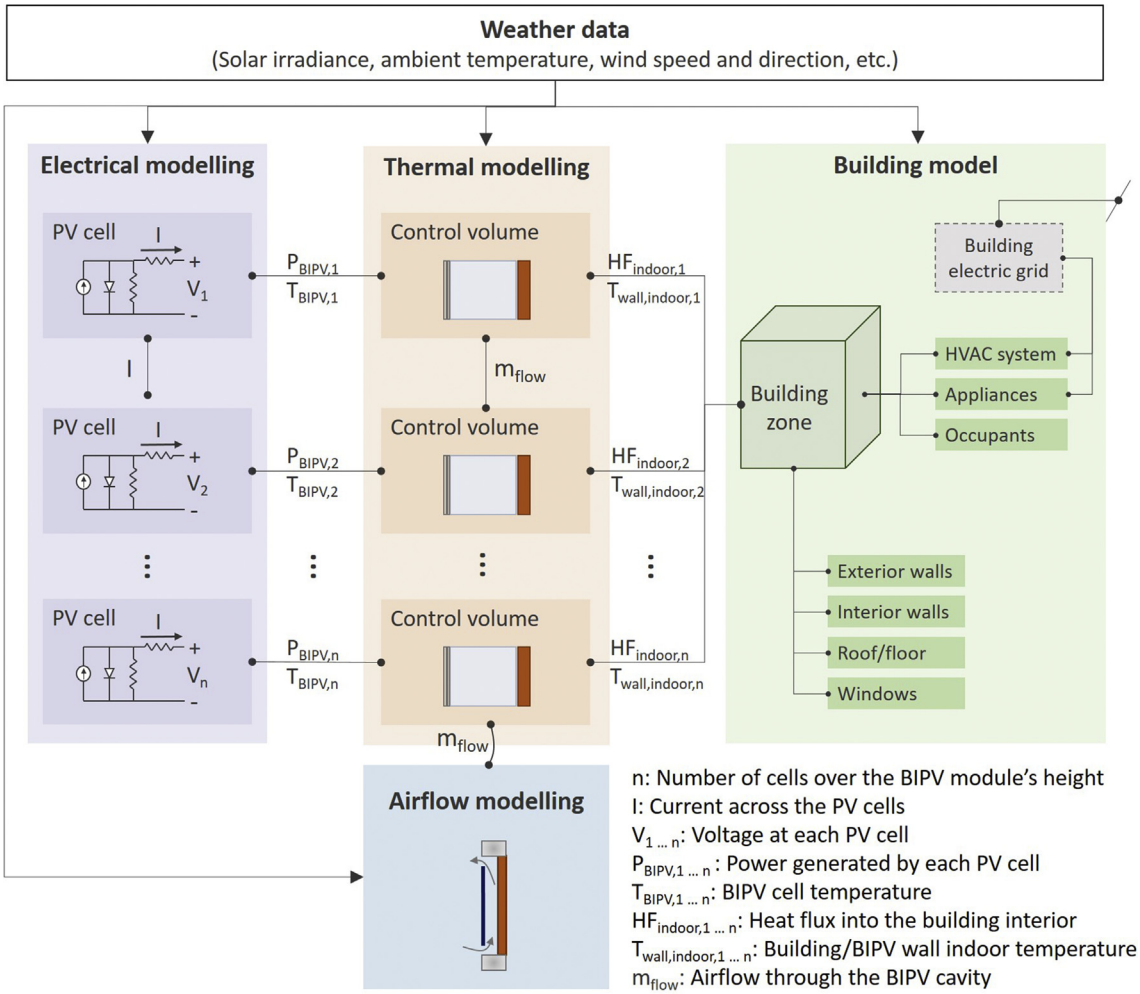

Fig. 1. Schematic representation of the multi-physics BIPV model (adapted from Ref. [32]).

yet been decided. In this case, the analyst should look at the inputs as design variables with equal probability (uniform distribution), rather than natural uncertainties (normal distributions).

The objective of this paper aligns with this second case. Therefore, the SA presented in this paper considers inputs that can be modified (to some extend) by changing the BIPV design. Although not related to the BIPV design, additional inputs concerning the exterior and indoor conditions are also considered in the SA to better understand the influence of the selected inputs under different operating conditions. The inputs selected for the SA are: (1) the exterior convective heat transfer coefficient, h_{ext} (associated with Q_{ext}), (2) the convective heat transfer coefficient between the PV module and the air inside the cavity, h_{PV} (associated with Q_{PV}), (3) the convective heat transfer coefficient between the building wall and the air inside the cavity, h_{wall} (associated with Q_{wall}), (4) the convective heat transfer coefficient at the building wall interior surface h_{indoor} (associated with Q_{indoor}), (5) the indoor temperature, T_{indoor}, (6) the airflow through inside the cavity, m_{flow}, (7) the plane-of-array (POA) solar irradiance reaching the BIPV module, I_{POA}, (8) the ambient temperature, T_{amb}, and (9) the temperature of the air entering the BIPV cavity, $T_{air,in}$. The reader is addressed to Fig. 2 to see how these inputs are defined in the multi-physics BIPV model. Note that in this paper h represents convective heat transfer coefficients, in contrast to h_c or CHTC commonly used in the literature.

Another important aspect of a SA is the definition of the outputs. In this work, the main indicators are the BIPV power at the maximum power point (MPP) and BIPV cell temperature at the top of the module. These two outputs represent the electrical and thermal performance of the BIPV module. Additional indicators considered in this paper are the heat flux through the building wall and the building wall temperature (at both cavity and indoor sides, also at the top of the BIPV module). Note that due to natural ventilation, the BIPV cell temperature varies over the height of the module, increasing from the bottom to the top. Here, the focus is on the most critical cell temperature occurring at the top.

3.2. Inputs range and distribution

This section describes each input in detail and how their range is defined. The exterior heat transfer coefficient h_{ext} results from the combination of forced and natural convection at the exterior BIPV surface. Forced convection is related to the wind flow around the building while natural convection is related to buoyancy forces due to temperature differences. Forced convection is relatively stronger than natural convection, as highlighted in Ref. [13]. Therefore, the range for h_{ext} is defined based on forced convection related to wind effects. The works in Refs. [27,28] reveal that the range of variation for (surface-average) h_{ext} is as broad as 0–100 W/(m^{2}K) for a wind speed at 10 m height between 0 and 15 m/s (depending on the h_{ext}

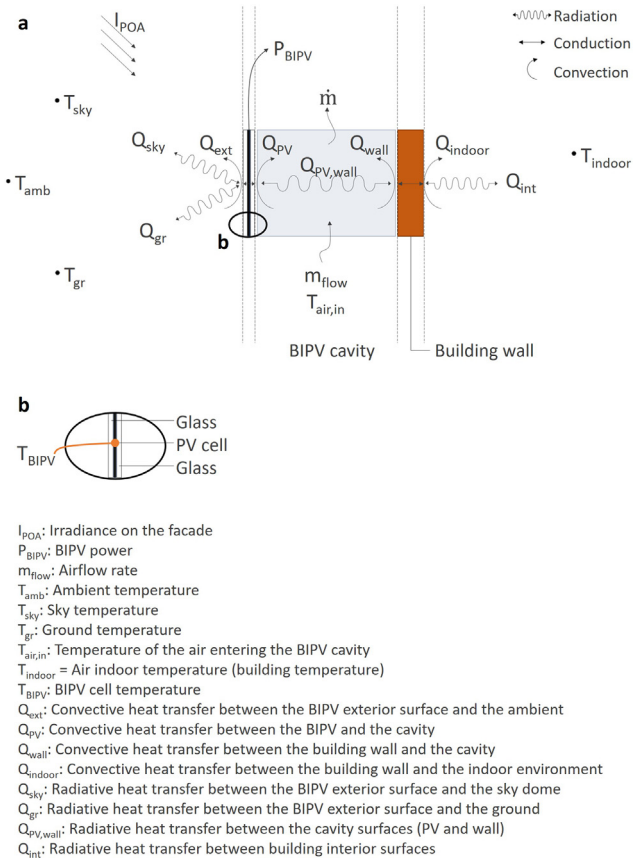

Fig. 2. Schematics of (a) a BIPV control volume element and (b) the exterior layers of the BIPV module (adapted from Ref. [32]).

model). In addition, the study in Ref. [35] shows that such large h_{ext} variation occurs over the same building facade, with the top corners of the facade experiencing h_{ext} values up to six times larger compared to the bottom middle of the facade. For a high-rise building and a wind speed at 10 m height of 3 m/s, h_{ext} varies from about 8 W/(m^{2}K) at the bottom/middle to about 55 W/(m^{2}K) at the top corners; for a wind speed of 5 m/s, the variation can be as large as 13–85 W/(m^{2}K). Considering these indicative values, the h_{ext} range is defined as 1–100 W/(m^{2}K).

As for natural convection in cavities (h_{PV} and h_{wall} in Fig. 2), the review presented in Ref. [13] indicates that convective heat transfer coefficients are expected to be in a range from 1 to 15 W/(m^2 K). The limits for h_{PV} and h_{wall} are chosen to correspond to this range. The experimental study conducted in Ref. [36] indicates that values around 5 W/(m^{2}K) are indeed realistic for natural convection in cavities. Higher values may represent enhanced heat transfer techniques, such as fins or heat pipes.

The indoor conditions are defined by two inputs, i.e. the indoor temperature (T_{indoor}) and the convective heat transfer at the internal surface of the building wall (h_{indoor} in Fig. 2). The T_{indoor} range is defined as 18–26 °C to represent diverse indoor conditions. The research in Ref. [37] shows that interior convective heat transfer coefficients may vary from 0.5 to 5 W/(m^{2}K) for a temperature difference of about 6 °C (between the building surface temperature and indoor temperature). This is the range adopted for h_{indoor} in this work.

The airflow rate (m_{flow}) in naturally ventilated elements depends on the pressure characteristics of the building element (e.g. how large are the cavity openings) and on the driving pressure differential (buoyancy and wind effects). Experimental data presented in Refs. [38,39] shows that the airflow rate in naturally ventilated BIPV modules is generally below 0.5 kg/s. In this paper, a larger range of 0.005–1 kg/(sm) is taken for m_{flow}. The larger values may represent mechanically ventilated cavities. Also note that the airflow rate is treated per unit width of BIPV module, i.e. kg/(sm), with the BIPV width equal to 1 m.

Concerning the weather conditions, the plane-of-array irradiance (I_{POA}) and the ambient temperature (T_{amb}) are selected as inputs in this work. I_{POA} is taken within a large range from 400 to 1200 W/m^2, with relatively lower values to represent facades partially shaded or less-exposed orientations, and relatively higher values to represent well-exposed facades. Similarly, T_{amb} is taken within a broad range from 5 to 35 °C to represent diverse ambient conditions.

Finally, a study on double skin facades has shown that the temperature of the air entering the cavity ($T_{air,in}$) can be notably higher than the ambient temperature (up to 15 °C) [40]. Measurements in the BIPV setup used to validate the BIPV model also indicate that the inlet temperature can be significantly higher than the ambient temperature. This temperature raise is due to local heat transfer occurring at the openings, which depends on the solar radiation and the cavity geometry. In this study, the $T_{air,in}$ range is taken between 0 and 10 °C higher ($\Delta T_{air,in}$) than the ambient temperature (T_{amb}). Note that the results are reported for $T_{air,in}$.

Table 2 summarises the inputs for the SA and their respective minimum and maximum values. To understand how the BIPV model behaves at representative conditions for sunny days, the simulations are performed for a second and a third combination of parameters (Cases 2 and 3), which define a narrower range for some of the parameters, as presented in Table 2. In particular, Case 2 narrows the range of the weather conditions to emulate representative operating conditions for BIPV facades, i.e. irradiance around 800 W/m^2 and ambient temperature between 20 and 25 °C. Because h_{ext} cannot be directly controlled by the BIPV designer, Case 3 is defined to represent less favourable exterior convective heat transfer conditions, i.e. h_{ext} lower than 30 W/(m^{2}K). Under lower h_{ext}, the impact of cavity ventilation on the BIPV performance can be investigated. Finally, as explained previously, since this paper employs SA methods with a design perspective, a uniform distribution has been assigned to all the inputs. This means that any value within the defined ranges is equally probable.

3.3. Generation of the input vectors

The third step of the methodology is to generate the input vectors, which can be done through the various sampling techniques available in the literature [25]. Some SA methods are associated to specific sampling techniques, as it is the case for eFAST (Fourier amplitude sensitivity testing) and Sobol analysis. For eFAST, the sampling technique described in Ref. [31] is used with N = 1000 and M = 4, where N is the number of samples and M is the interference parameter, resulting in 9000 combinations. For the Sobol analysis, also N = 1000 samples have been generated using the Saltelli's sampling technique, as described in Ref. [31], resulting in 20,000 simulations. The Saltelli's samples are also used for the generation of scatter plots and the calculation of regression coefficients (explained in Section 3.5).

3.4. Generation of the output vectors

The output vectors are generated from the multi-physics BIPV model as illustrated in Fig. 4b. Every input vector has a corresponding output vector. As mentioned previously, the model outputs considered in this work are: BIPV temperature, BIPV power, building wall temperatures, and heat flux into the building. Note

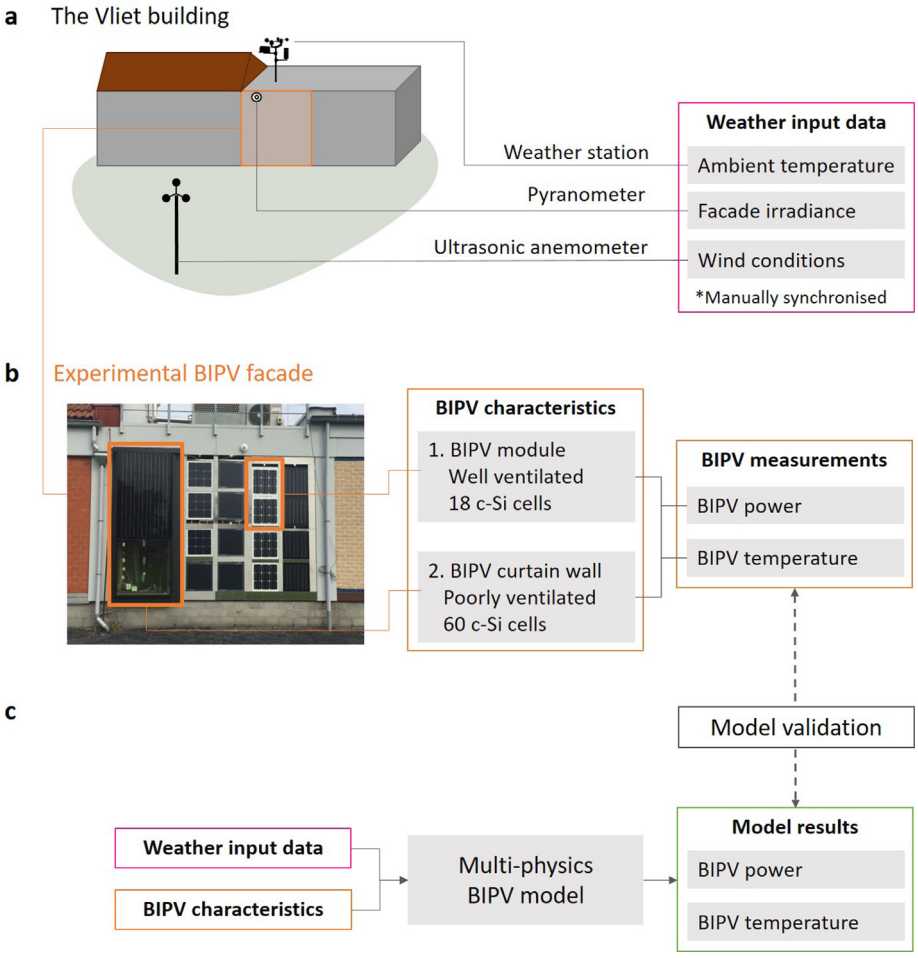

Fig. 3. (a) Schematic of the Vliet test building and weather monitoring. (b) The experimental BIPV facade and monitoring of the BIPV performance. (c) BIPV model inputs and outputs, indicating how the model validation is carried out.

Table 1
Material properties of the BIPV module used in the simulations.

	Glass	PV cell	Building wall
Thickness [m]	0.003	0.0001	0.15
Thermal conductivity [W/mK]	0.96	710	0.036
Heat capacity [J/kgK]	750	710	840
Density [kg/m^3]	2500	2330	110
Short-wave emissivity [–]	0.95	–	–
Long-wave emissivity [–]	0.9	–	0.8

that this step is a good instrument of model verification [24]. Indeed, the inspection of the results shows that the multi-physics BIPV model provides consistent outputs for all input vectors.

3.5. SA methods

Global SA methods are classified in four groups [22], as follows: regression, screening-based, variance-based, and meta-model sensitivity analysis. This paper focuses on regression coefficients and variance-based methods (eFAST and Sobol analysis). Scatter plots are also used for visual insight into the results.

Regression methods quantify the extent to which a given input changes the target output, describing both the strength and the direction of a relationship. Regression coefficients are easy to compute and to interpret. Two commonly used correlation measures are the Pearson's correlation coefficient, which evaluates the linear relationship between one input and the target output, and the Spearman's correlation coefficient, which evaluates their monotonic relationship, linear or non-linear. While the linear relationship implies a constant variation rate between input and output, a monotonic behaviour means that the output either increases or decreases with increasing the input.

Both eFAST and Sobol analysis belong to the variance-based family. Their main advantage is that they can be applied to any model, linear or non-linear [22,23]. These methods associate the variability of the outputs to the inputs [41]. The two main sensitivity measures are the first order (individual) and total effects. The individual effects account for the contribution of each input factor to the output variability. Total effects compute the total contributions of a given input to the output variance, including both individual and higher-order effects from interactions among inputs. The difference between first and total order measures corresponds, thus, to the effect of interactions among inputs.

The difference between eFAST and Sobol analysis lies on the numerical computation of the multidimensional integrals of the model necessary for the calculation of the sensitivity indices [42]. The two methods are considered in this paper only for verification purposes. In SALib [31], the eFAST implementation is based on [41,43], and the Sobol analysis implementation is based on [44–46].

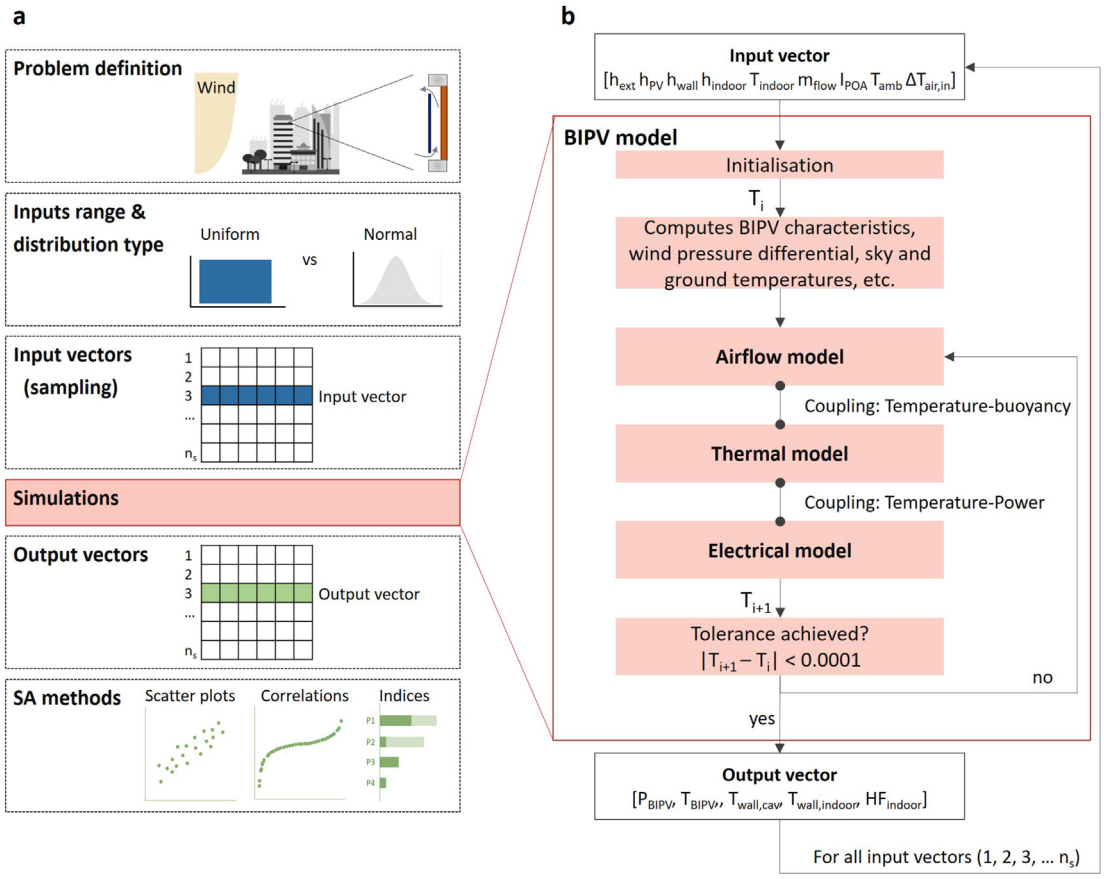

Fig. 4. (a) Work flow for the SA, and (b) detailed work flow illustrating how the BIPV model is used in the SA framework.

4. Results

4.1. BIPV performance

4.1.1. Scatter plots

Scatter plots are used as a starting point to visually explore the relationship between inputs and outputs. Fig. 5 shows the scatter plots of BIPV temperature (T_{BIPV}) and power (P_{BIPV}) for Case 1 (see Table 2). These plots show that T_{BIPV} and P_{BIPV} respond differently to variations in the model inputs. Firstly, it can be observed that T_{BIPV} tends to decrease with increasing h_{ext}. This trend is expected since a higher h_{ext} means that more heat is dissipated to the exterior environment. In contrast, T_{BIPV} tends to increase with increasing T_{amb} and $T_{air,in}$. Physically, these trends also make sense: a higher T_{amb} means that less heat is dissipated to the exterior and a higher $T_{air,in}$ means that the air enters the BIPV cavity at higher temperatures, reducing the amount of heat dissipated to the cavity due to the smaller temperature difference between T_{BIPV} and $T_{air,in}$. For the remaining inputs, the spread in T_{BIPV} is large and no clear can be identified (i.e. the spread is more uniformly distributed). Secondly, it can be observed that P_{BIPV} is significantly affected by I_{POA} (also expected, since increasing irradiance leads to higher power generated). Again, for the remaining inputs, the P_{BIPV} results are uniformly scattered and no clear trend is observed.

Given the broad ranges selected for Case 1, a first practical interpretation of these results is to look at the variations of T_{BIPV} and P_{BIPV} as the operating space for naturally ventilated BIPV facades. T_{BIPV} predictions mainly vary within 20 °C and 50 °C, but values as low as 10 °C and as high as 90 °C are observed. P_{BIPV} values lie mostly between 0.4 and 1.2 W/W_P ($P_{STC} = 244$ W_P). This means that depending on the input values, the BIPV module can perform rather poorly at around 0.4 W/W_P or it can perform rather satisfactorily up to 1.2 W/W_P. As indicated in Fig. 5c, higher P_{BIPV} values result from the combination of high irradiance (above 1000 W/m^2) and lower T_{BIPV} (below 25 °C).

Fig. 6 presents the scatter plots for Case 2, in which the variations of I_{POA}, T_{amb} and $T_{air,in}$ are limited. Case 2 could represent a given moment in time, in which the weather conditions are defined. The plots for I_{POA}, T_{amb} and $T_{air,in}$ are not shown here for the sake of conciseness, but their effect will be discussed in Section 4.1.2. A first observation is that the influence of h_{ext} on T_{BIPV} is now more evident, confirming the behaviour observed in Fig. 5. The spread in the results is significantly reduced compared to the other inputs (the pattern of points resemble a thick line), indicating a non-linear relationship between h_{ext} and both T_{BIPV} and P_{BIPV}. An increasing h_{ext} results in lower T_{BIPV} and higher P_{BIPV}. While this

Table 2
Inputs and corresponding ranges for Case 1 and Case 2.

		Case 1		Case 2		Case 3	
		Min	Max	Min	Max	Min	Max
h_{ext}	$W/(m^2K)$	1	100	1	100	1	30
h_{PV}	$W/(m^2K)$	1	15	1	15	1	15
h_{wall}	$W/(m^2K)$	1	15	1	15	1	15
h_{indoor}	$W/(m^2K)$	0.5	5	0.5	5	0.5	5
T_{indoor}	°C	18	26	20	22	20	22
m_{flow}	kg/(sm)	0.005	1	0.005	1	0.005	1
I_{POA}	W/m^2	400	1200	790	810	790	810
T_{amb}	°C	5	35	20	25	20	25
$\Delta T_{air,in}$	°C	0	10	0	10	0	10

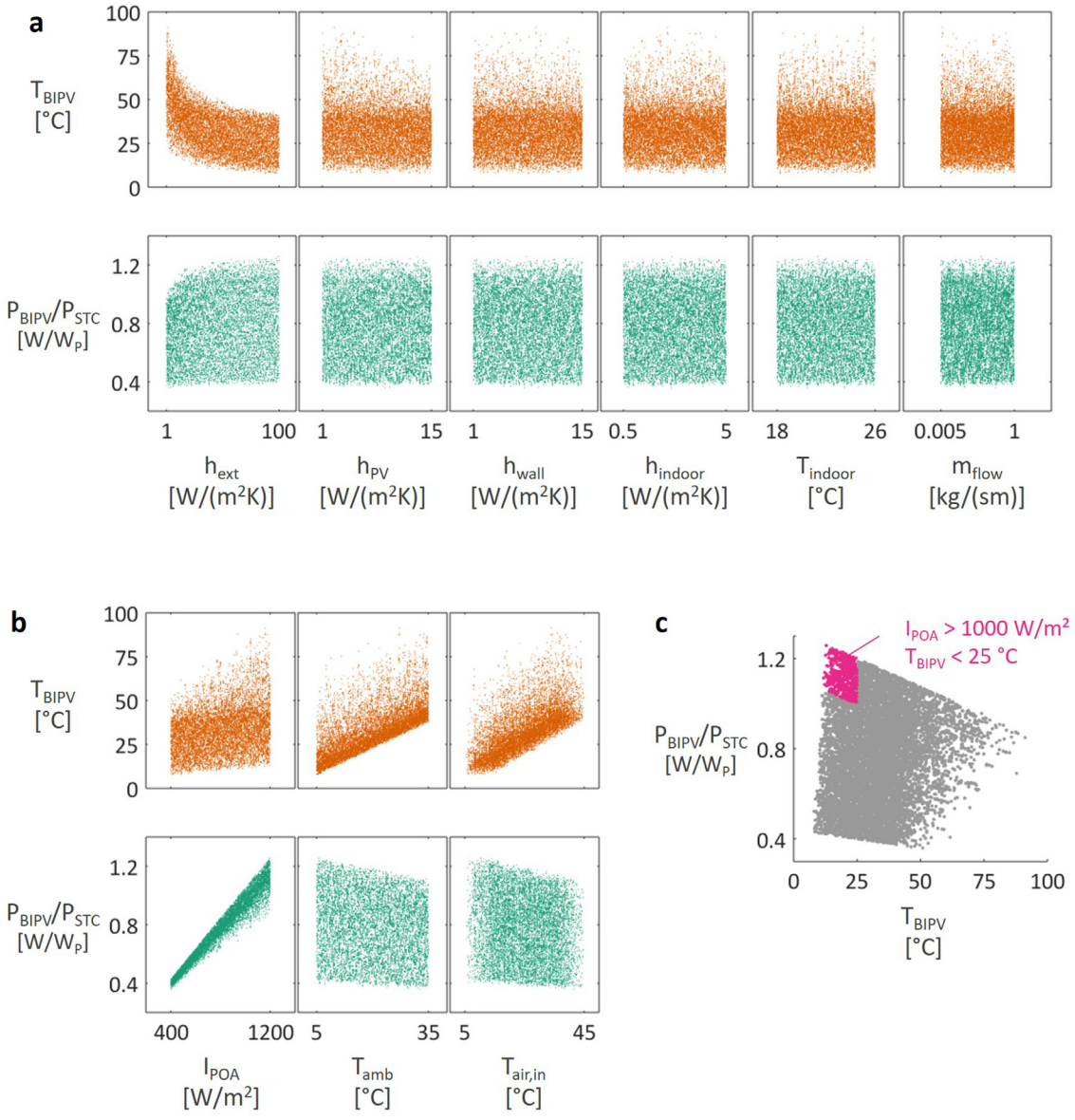

Fig. 5. Scatter plots for Case 1: a) Heat transfer and airflow inputs; b) Weather inputs; c) P_{BIPV} as a function of T_{BIPV}, highlighting points with I_{POA} > 1000 W/m^2 and T_{BIPV} < 25 °C (20,000 simulations).

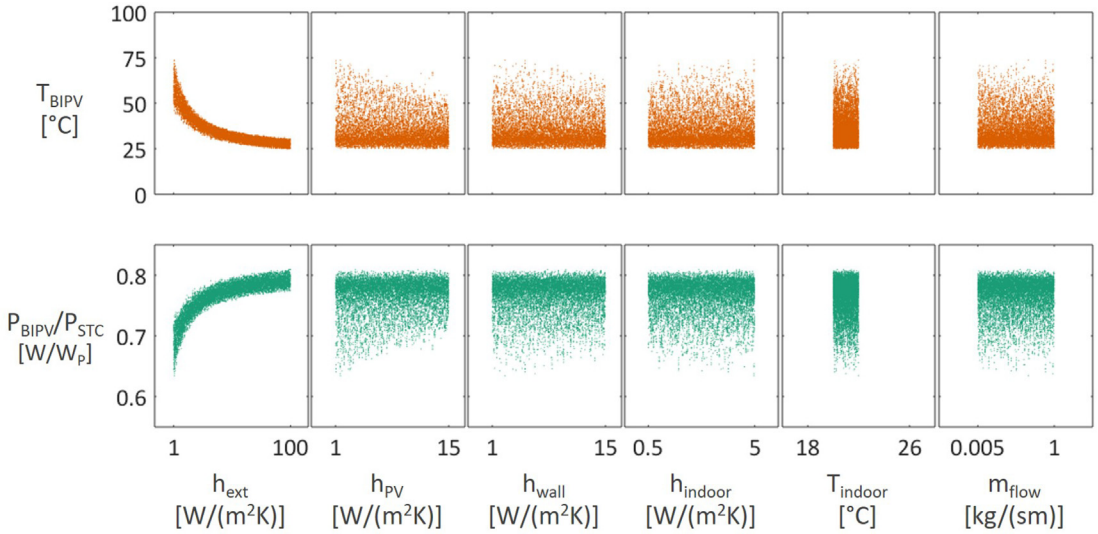

Fig. 6. Scatter plots for Case 2 (20,000 simulations).

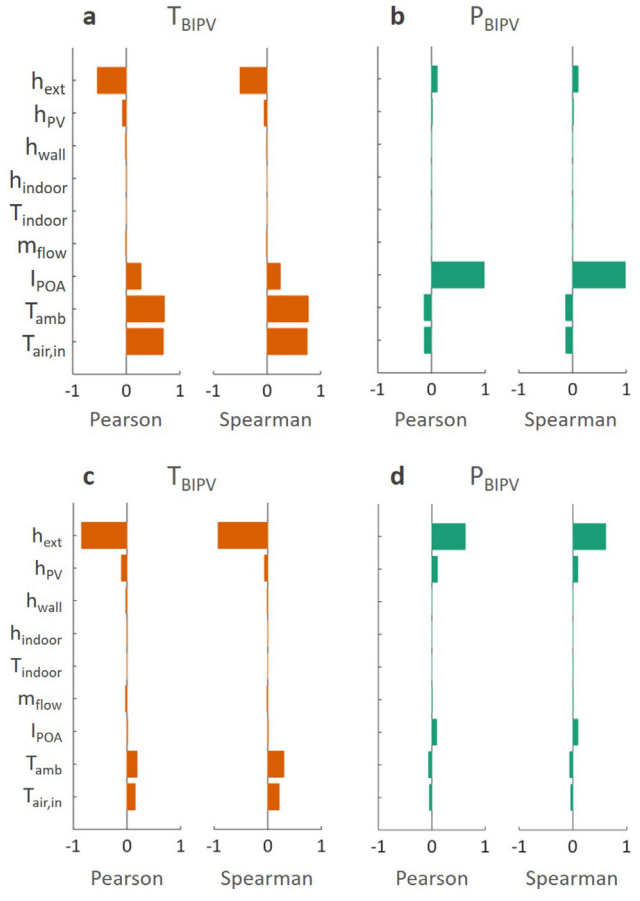

Fig. 7. Correlation coefficients for temperature (T_{BIPV}) and power (P_{BIPV}) for a,b) Case 1 and c,d) Case 2 (20,000 simulations).

trend is expected, the plot shows the shape of this relationship. It shows that variations in T_{BIPV} and P_{BIPV} with h_{ext} are stronger for h_{ext} below approximately 30 W/(m^2K). For h_{ext} higher than 30 W/(m^2K), T_{BIPV} and P_{BIPV} vary much less and tend to constant values (T_{BIPV} tends to 25 °C and P_{BIPV} tends to 0.8 W/W_P). Also the influence of h_{PV} is more evident now: a h_{PV} close to 15 W/(m^2K) can reduce the BIPV temperature from about 75 to 50 °C and increase the power from around 0.65 to above 0.7 W/W_P (i.e. approximately from 150 to 175 W).

In addition, the operating ranges of temperature and power change significantly compared to Case 1, with Case 2 presenting T_{BIPV} mostly within 25 °C and 50 °C and P_{BIPV} within 0.75 and 0.8 W/W_P (note that Figs. 5 and 6 have different scales for P_{BIPV}). Interestingly, T_{BIPV} still varies significantly in Case 2, despite the narrow variation ranges defined for irradiance (I_{POA} between 790 and 810 W/m^2) and ambient temperature (T_{amb} between 20 and 25 °C). This large T_{BIPV} variation includes all possible combinations of inputs, which indicates that some input combinations provide better cooling conditions. For instance, in Fig. 6, either a higher h_{ext} or a higher h_{PV} leads to lower T_{BIPV}.

4.1.2. Correlation coefficients

The correlation coefficients obtained from the regression method are presented in Fig. 7a and b and Fig. 7c and d for Case 1 and Case 2, respectively, for both for temperature (T_{BIPV}) and power (P_{BIPV}). A negative sign means an inverse relationship between the given input and output. The p-values related to the correlation coefficients are presented in Table 3.

Table 3
p-values for Case 1 and Case 2.

	Case 1				Case 2			
	Pearson		Spearman		Pearson		Spearman	
	T_{BIPV}	P_{BIPV}	T_{BIPV}	P_{BIPV}	T_{BIPV}	P_{BIPV}	T_{BIPV}	P_{BIPV}
h_{ext}	0.00	0.00	0.00	0.00	0.00	0.00	0.00	0.00
h_{PV}	0.00	0.00	0.04	0.04	0.00	0.00	0.00	0.00
h_{wall}	0.04	0.27	0.84	0.87	0.01	0.09	0.01	0.12
h_{indoor}	0.59	0.99	0.81	0.93	0.49	0.79	0.52	0.55
T_{indoor}	0.83	0.82	0.57	0.55	0.81	0.94	0.98	0.87
m_{flow}	0.09	0.09	0.63	0.64	0.00	0.06	0.01	0.25
I_{POA}	0.00	0.00	0.00	0.00	0.11	0.15	0.00	0.00
T_{amb}	0.00	0.00	0.00	0.00	0.00	0.00	0.00	0.00
$T_{air,in}$	0.00	0.00	0.00	0.00	0.00	0.00	0.00	0.00

For Case 1, the correlation coefficients and p-values indicate that T_{BIPV} predictions are correlated with h_{ext}, I_{POA} and T_{amb} and $T_{air,in}$ (Fig. 7a), in agreement with the observations from the scatter plots in Figs. 5 and 6. The influence of $T_{air,in}$ highlighted in Ref. [47] is thus confirmed. For the other inputs, the p-values are inconclusive (higher than 0.05). For P_{BIPV} predictions, strong correlations with I_{POA} are observed (Fig. 7b). In addition, the correlation coefficients reveal some influence of h_{ext}, T_{amb} and $T_{air,in}$ on P_{BIPV} (Fig. 7b). Again, for the other inputs, the p-values are mostly inconclusive.

For Case 2, the correlation coefficients confirm that T_{BIPV} is highly correlated to h_{ext} (Fig. 7c). With a Pearson's coefficient of −0.8463, their relationship cannot be considered linear, but with a Spearman's coefficient of −0.9251, it can be assumed fairly monotonic. h_{PV} also presents some correlation, but of less importance. The influence of I_{POA}, T_{amb} and $T_{air,in}$ is obviously reduced since their variation range is limited. The coefficients for P_{BIPV} present a similar trend as observed for temperature predictions, with strongest influence of h_{ext} (see Fig. 7c and d). Note that the difference between Cases 1 and 2 is more pronounced for P_{BIPV} results: in Case 1, P_{BIPV} mostly correlates with I_{POA} (Fig. 7b), while in Case 2, P_{BIPV} mostly correlates with h_{ext} (Fig. 7d).

Finally, it is important to highlight that, although T_{BIPV} and P_{BIPV} predictions are both significantly correlated with h_{ext} in Case 2, the magnitude of the correlations is lower for P_{BIPV}: Pearson's and Spearman's coefficients decrease from −0.8463 and −0.9251 for T_{BIPV} to 0.8293 and 0.8764 for P_{BIPV}. Such result is expected, since the temperature is directly influenced by h_{ext}, while power is indirectly affected by h_{ext} (i.e. h_{ext} influences the temperature, which in turn affects the power output).

4.1.3. eFAST and Sobol analysis

The eFAST and Sobol analysis provide sensitivity indices that represent individual (first order) and total (order) effects of the inputs on the variability of the outputs, as shown in Figs. 8 and 9 for both Cases 1 and 2. Overall, Sobol results are in agreement with eFAST, which in turn are consistent with the observations in the previous sections based on scatter plots and correlation coefficients. h_{ext} has an important influence on the T_{BIPV} variation for both Cases 1 and 2 (Fig. 8a,c and 9a,c). For Case 2, h_{ext} also dominates the variation in P_{BIPV} (Figs. 8c and 9c). In addition, the sensitivity indices show that individual effects dominate the outputs variability. The influence of interactions between inputs is slightly more pronounced for T_{BIPV} in Case 1, in particular for h_{ext} and I_{POA}, due to their larger variation ranges (Figs. 8a and 9a).

4.1.4. Influence of cavity ventilation

The results presented so far have shown that the influence of the inputs related to the cavity ventilation is smaller compared to the other inputs, particularly due to the dominance of h_{ext}. However,

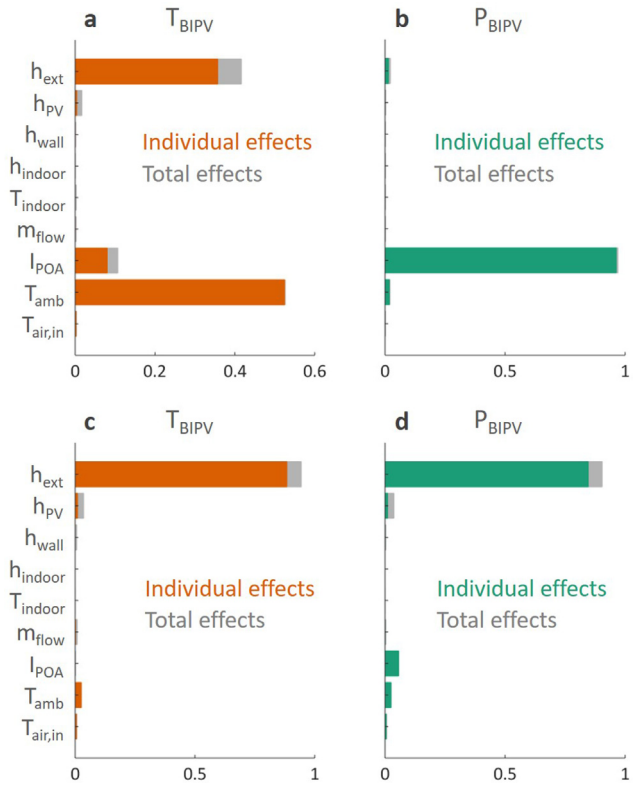

Fig. 8. eFAST analysis: Individual and total effects for temperature (T_{BIPV}) and power (P_{BIPV}) predictions for a,b) Case 1 and c,d) Case 2.

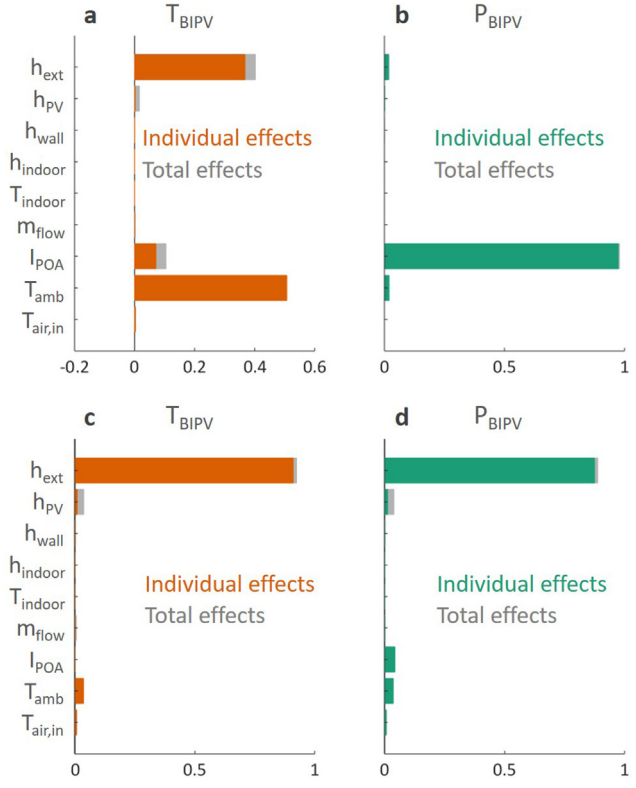

Fig. 9. Sobol analysis: Individual and total effects for temperature (T_{BIPV}) and power (P_{BIPV}) predictions for a,b) Case 1 and c,d) Case 2.

the results have also shown that the relationship between inputs and outputs is strongly dependent on the range of the inputs. The research question here is how the model behaves when the h_{ext} range is limited and whether cavity ventilation is important under such conditions. For this analysis, this section focuses on Case 3 as defined in Table 2. In this scenario, the variation range of the exterior convective heat transfer coefficient is significantly reduced from 0–100 W/(m^{2}K) to 0–30 W/(m^{2}K) (note that this is the only difference between Cases 2 and 3).

Fig. 10 shows the scatter plots of P_{BIPV} as a function of T_{BIPV}, highlighting combinations where h_{ext} is below 30 W/(m^{2}K) (results from Case 1). This reduction in exterior heat dissipation shifts the results towards higher T_{BIPV}, up to 90 °C, and generally lower P_{BIPV}, below 1.2 W/W$_P$. Next, Fig. 11 presents the correlation coefficients and eFAST indices obtained for T_{BIPV} for Case 3 (again, Sobol indices are similar to eFAST indices). These results show that at lower h_{ext} conditions, the influence of inputs related to cavity ventilation (i.e. h_{PV} and m_{flow}) becomes more important for the T_{BIPV} predictions (compared to Case 2 in Fig. 7). The P_{BIPV} results are not significantly affected and, therefore, are not presented here.

4.2. Building performance

Fig. 12 presents the scatter plots for the building wall temperature at the cavity side ($T_{wall,cav}$), the building wall temperature at the building indoor side ($T_{wall,\ indoor}$), and the heat flux into the building (HF_{indoor}) for Case 1. In general, $T_{wall,cav}$ remains below 40 °C, $T_{wall,\ indoor}$ remains below 30 °C, while HF_{indoor} varies mostly within −5 to +10 W/m^2 (positive sign indicates heat flux into the building). Note that the scatter plots for $T_{wall,cav}$ are similar to the ones obtained for T_{BIPV} (Fig. 5), but $T_{wall,cav}$ exhibits somewhat lower temperature values, mostly in the range of 15–40 °C.

The correlation coefficients are presented in Fig. 13 for $T_{wall,cav}$, HF_{indoor} and $T_{wall,indoor}$, for Cases 1 and 2. Table 4 presents the respective p-values. For Case 1, both $T_{wall,cav}$ and HF_{indoor} exhibit stronger correlations with T_{amb} and $T_{air,in}$ (Fig. 13a and b), while $T_{wall,indoor}$ mostly correlates with T_{indoor}, as expected (Fig. 13c). Again, from Case 1 to Case 2, h_{ext} becomes a more important input for the three indicators (Fig. 13a,b,c compared to d,e,f). These results demonstrate that variations in h_{ext} also affect the building performance, in agreement with results presented in Refs. [28,48,49]. For the $T_{wall,indoor}$, the influence of h_{indoor} also becomes more important (Fig. 13f).

4.2.1. Influence of the building wall thermal resistance

The results presented so far correspond to a well insulated BIPV module with a thermal resistance $R_{wall} = 6.25$ (m^{2}K)/W (see Table 1

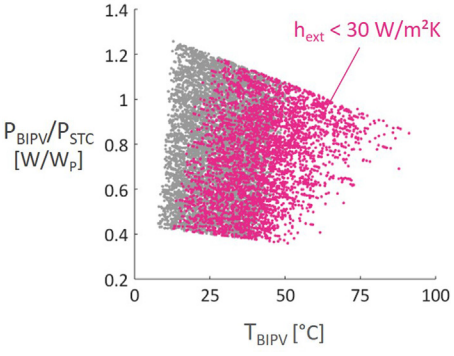

Fig. 10. P_{BIPV} as a function of T_{BIPV}. Results for which h_{ext} < 30 W/(m^{2}K) are highlighted (Case 1, 20,000 simulations).

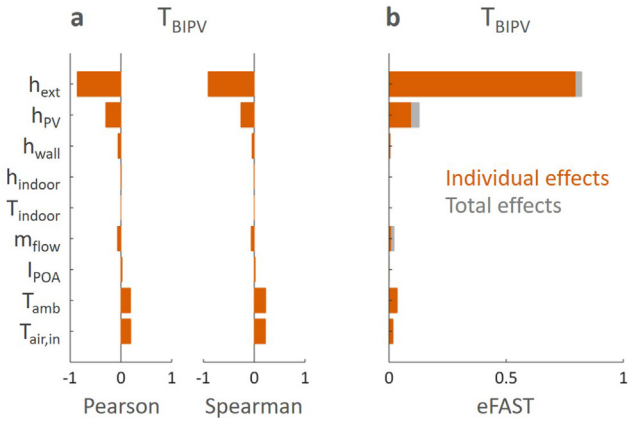

Fig. 11. T_{BIPV} results for Case 3 (20,000 simulations): a) Pearson's and Spearman's correlation coefficients and b) eFAST indices.

for the thermal properties). This thermal resistance value is taken as reference. Here, the building wall thermal resistance is reduced by a factor of three (i.e. $R_{wall}/3 = 2.08$ $(m^2K)/W$), broadening the scope of the paper to represent buildings that are less insulated. Fig. 14 presents the scatter plots for a building wall with $R_{wall}/3$ for Case 1. Only the heat flux into the building HF_{indoor} and the building wall temperature at the indoor surface $T_{wall,indoor}$ are shown. The building wall thermal resistance barely affects the BIPV temperature and power, which are therefore omitted. Compared to the reference case in Fig. 12, the results in Fig. 14 are slightly more spread.

To gain further insight on the influence of the building wall thermal resistance, the Sobol indices are calculated for $T_{wall,indoor}$ and HF_{indoor} for Case 1. These results are presented in Fig. 15. For HF_{indoor}, the building wall thermal resistance does not affect the Sobol indices significantly (Fig. 15a,c). This means that the HF_{indoor} response to changes in the inputs is not affected by the building wall thermal resistance. Note that the HF_{indoor} magnitude does change with the thermal resistance (will be discussed later). For $T_{wall,indoor}$, the Sobol indices indicate that the influence of T_{indoor} decreases when the thermal resistance is reduced to $R_{wall}/3$, while the influence of h_{ext}, h_{indoor} and T_{amb} becomes more pronounced (Fig. 15b,d). In addition, the effect of interactions between inputs (represented by the difference between individual effects and total effects) is larger for $R_{wall}/3$ (Fig. 15d). In particular, the total effects caused by variations in h_{indoor} and T_{amb} become more important.

Although the Sobol indices for HF_{indoor} are not affected by the building wall thermal resistance, the HF_{indoor} magnitude changes significantly, as shown in Fig. 16. As expected, the heat flux into the building interior increases significantly when the building wall thermal resistance is reduced to $R_{wall}/3$. The average HF_{indoor} increases from 1.6 W/m^2 to 4 W/m^2. The limits of the histograms are also different. For the highly insulated case, the minimum and maximum heat fluxes are −5 and 15 W/m^2, respectively, while for the less insulated condition, these values are −14 and 38 W/m^2.

5. Discussion

A first general remark concerns the dependency of the SA results on the variation ranges selected for the inputs, which is an intrinsic characteristic of such approaches. Rather than a limitation, this particularity provides an opportunity for evaluating the model response to different input ranges and distributions. In fact, the SA framework proposed here was developed to enable the fast modification of the inputs, their distributions and ranges. This paper investigates three cases, starting with broader input ranges and reducing them progressively. Uniform distributions have been assigned to all inputs for the three cases. One possibility to be explored in future work is assigning normal distributions to the inputs to evaluate the uncertainty of the multi-physics BIPV model. In addition, the SA framework can be extended to include more inputs, such as the radiative heat transfer coefficients, the sky temperature (which now is 10 °C below the ambient temperature), and/or property materials (e.g. the emissivity of the glass layers in the PV module and the emissivity of the cavity wall). Future work could also investigate the influence of the material structure of the building wall.

A significant difference in the model response is observed between Case 1 and Cases 2 and 3, notably for power predictions. In Case 1, the input ranges are defined to account for diverse weather conditions as well as BIPV design parameters, which define the airflow rate and convective heat transfer conditions. Case 1 illustrates the operating space of naturally-ventilated BIPV facades. Under these conditions, the BIPV temperature is mostly affected by h_{ext}, I_{POA} and h_{amb}, while the power output is mostly affected by I_{POA}. By narrowing the variation ranges, Cases 2 and 3 demonstrate how the SA framework is used to investigate the BIPV behaviour under more specific conditions. In these two cases, h_{ext} is identified as the strongest input influencing the BIPV performance (i.e. cell temperature and power output). The influence of h_{ext} on the building performance indicators is also observed in Cases 2 and 3. By demonstrating that h_{ext} is an important parameter for both the BIPV and building performances, the findings in this work resonate with several studies that recommend the implementation of more advanced h_{ext} models in building performance simulations, e.g. Refs. [27–30,35,49,50].

From a modelling point-of-view, the findings in this work are relevant given the variability and uncertainty of h_{ext} models, as identified in Refs. [27,28,49]. The relationship between h_{ext} and BIPV performance indicates that at lower wind speeds, the choice for a certain h_{ext} model could lead to significant differences, given the spread in the predictions. In this case, an accurate h_{ext} model is needed, posing an additional challenge for BIPV modelling, since the wind flow around the building is highly complex in the built environment, in particular in dense urban areas. In contrast, since the spread in temperature and power predictions decreases with increasing h_{ext}, the uncertainty in the h_{ext} model becomes less important at higher h_{ext}, notably above 30 $W/(m^2K)$.

From a design perspective, the results presented here indicate that efforts to improve the ventilation conditions (i.e. airflow and/or convective heat transfer coefficients inside the BIPV cavity) may have a higher impact at lower h_{ext} (Case 3). The larger spread in the predictions at lower h_{ext} shows that the other inputs become more important at these conditions, which is in fact confirmed by Case 3. At higher values of h_{ext}, this factor dominates the predictions, reducing the effect of variations in the other inputs. The work in Ref. [51] has indeed shown that when the external convective heat transfer coefficient is high, the ventilation in the cavity becomes less important. In practice, cavity ventilation may be more important for BIPV modules operating in dense building clusters, due to the lower h_{ext} generally observed in these conditions [35,48]. Lower wind speeds also occur close to the ground, where a region of increased residence time of the air is present, leading to an increase in the local air temperature and a reduction in the local value of h_{ext} [35].

Still from a practical perspective, it should be noted that modifications in one design parameter may have consequences on the others. For example, the adoption of fins to enhance the heat transfer inside the cavity could increase the resistance to the flow, leading to lower airflow rates. The increased resistance could in

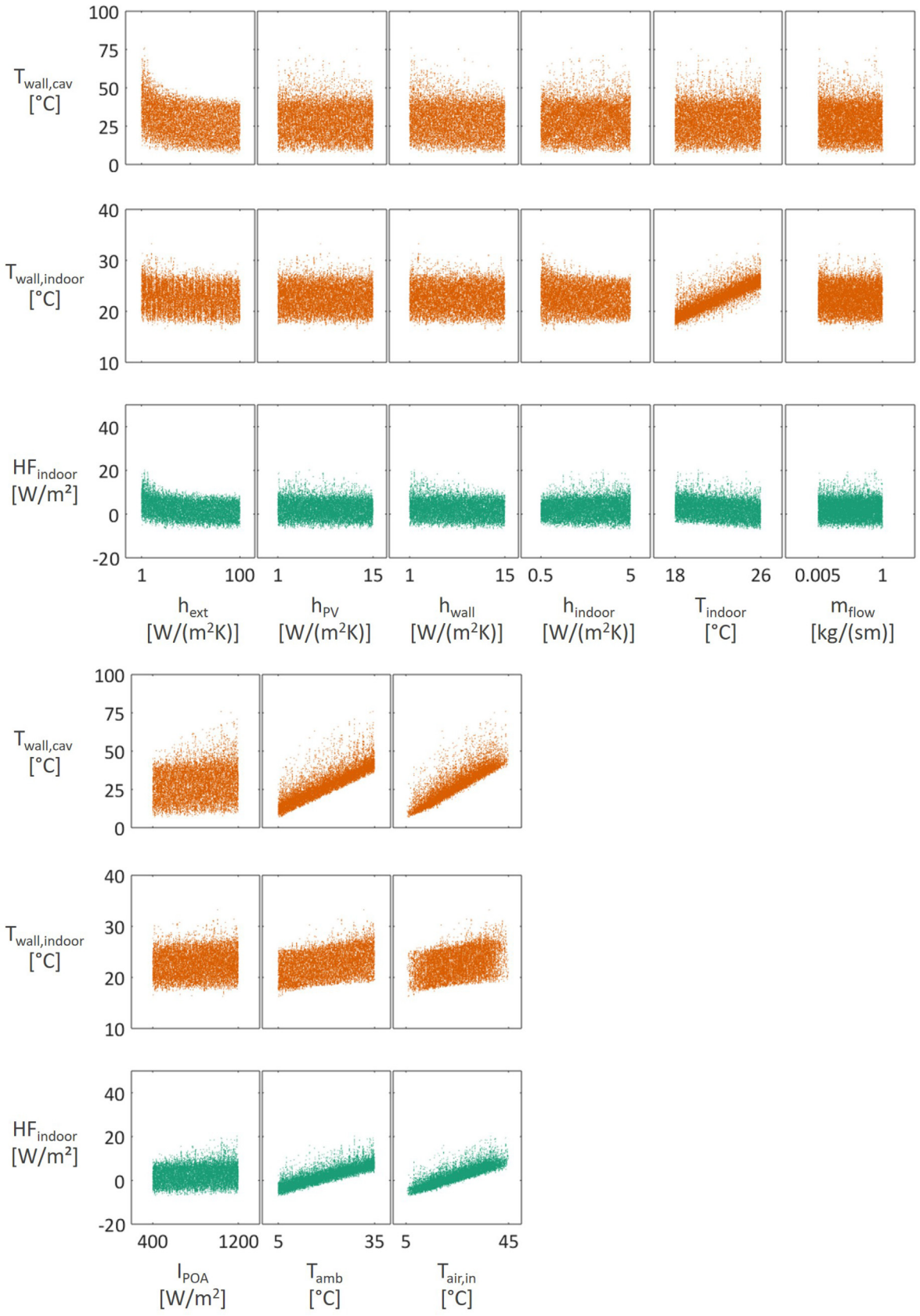

Fig. 12. Scatter plots for $T_{wall,\ indoor}$ and HF_{indoor} for Case 1 (20,000 simulations).

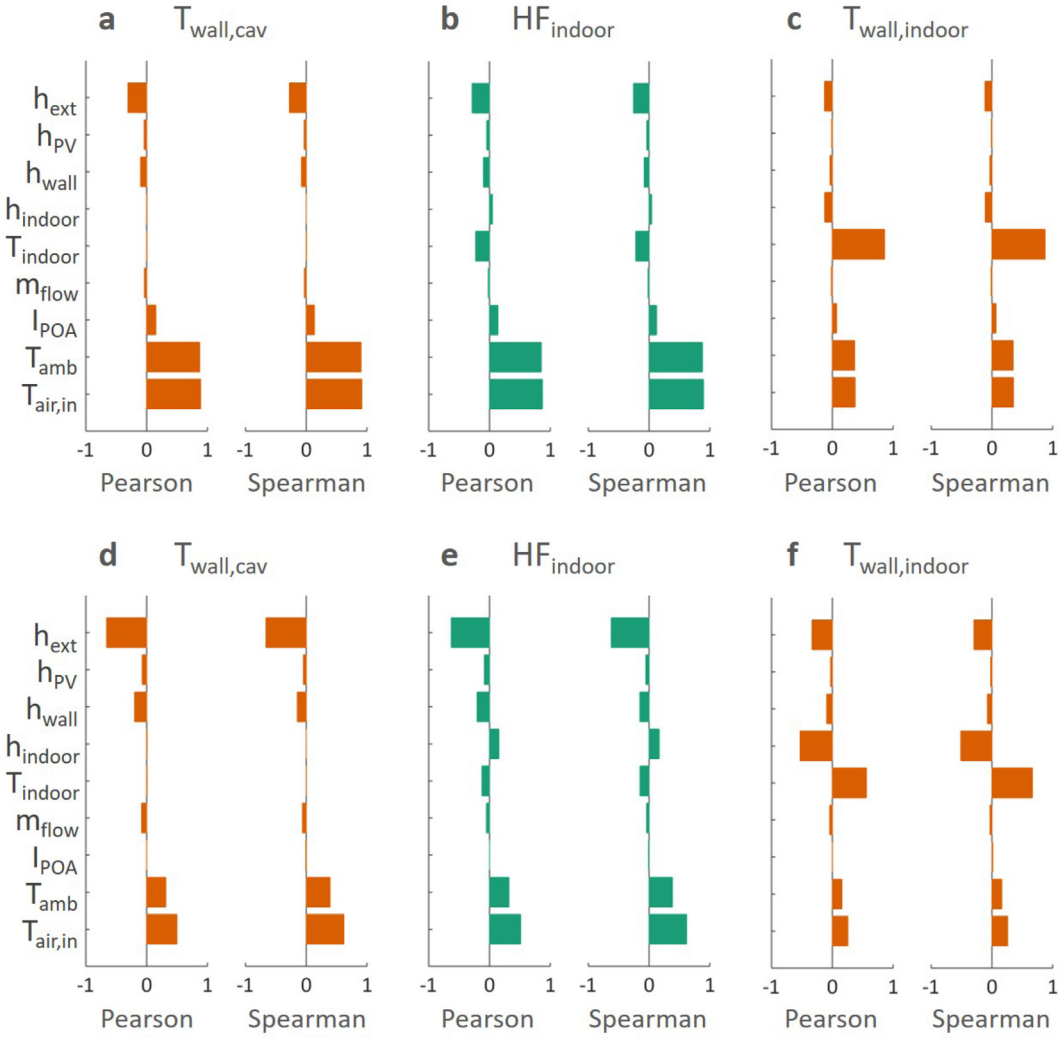

Fig. 13. Correlation coefficients for plots for $T_{wall,cav}$, $T_{wall,\ indoor}$ and HF_{indoor} for a,b,c) Case 1 and d,e,f) Case 2 (20,000 simulations).

Table 4
p-values for $T_{wall,cav}$, $T_{wall,indoor}$ and HF_{indoor} for Case 1.

	$T_{wall,cav}$		HF_{indoor}		$T_{wall,\ indoor}$	
	Pearson	Spearman	Pearson	Spearman	Pearson	Spearman
h_{ext}	0.00	0.00	0.00	0.00	0.00	0.00
h_{PV}	0.00	0.00	0.00	0.00	0.11	0.19
h_{wall}	0.00	0.00	0.00	0.00	0.00	0.00
h_{indoor}	0.63	0.93	0.00	0.00	0.00	0.00
T_{indoor}	0.53	0.61	0.00	0.00	0.00	0.00
m_{flow}	0.00	0.00	0.01	0.02	0.04	0.05
I_{POA}	0.00	0.00	0.00	0.00	0.00	0.00
T_{amb}	0.00	0.00	0.00	0.00	0.00	0.00
$T_{air,in}$	0.00	0.00	0.00	0.00	0.00	0.00

turn be compensated by increasing the size of the cavity openings, maintaining the same airflow rate. While the approach in this paper considers these combinations both feasible and equally probable (e.g. fins and larger openings, and no fins and smaller openings), detailed modelling techniques such as computational fluid dynamics (CFD) are more appropriate to investigate particular configurations. This effort is, however, beyond the scope of this paper, but will be considered in future studies. Nevertheless, this paper reveals the potential for reducing the BIPV temperature by about 25 °C and increasing the power output by about 25 W, only by improving h_{PV}.

Finally, the interaction between exterior and indoor environments is discussed. The SA results presented here show that inputs related to the indoor conditions (i.e. h_{indoor} and T_{indoor}) do not affect significantly the BIPV performance (temperature and power), regardless of the building thermal resistance. Therefore, in terms of BIPV performance, the BIPV module could be (thermally) decoupled from the building indoor conditions. However, this is not entirely the case for the total heat flux into the building interior and the building wall temperature on the inside. The heat flux remains sensitive to the same parameters for both building thicknesses, including h_{ext}. As expected, the heat flux magnitude also changes significantly when the building wall thermal resistance is reduced, affecting the cooling and heating loads of the building. For a reduced wall thermal resistance, the building wall temperature on the inside becomes more sensitive to inputs related to the exterior conditions, such as h_{ext} and T_{amb}. Moreover, the Sobol indices show that interactions between inputs also become more important, increasing the modelling complexity. These results corroborate the importance of simulating the BIPV module as part of the building envelope for an accurate representation of the thermal performance of the building, particularly in the case of a low thermal resistance between the PV and the building, as discussed in Refs. [52,53].

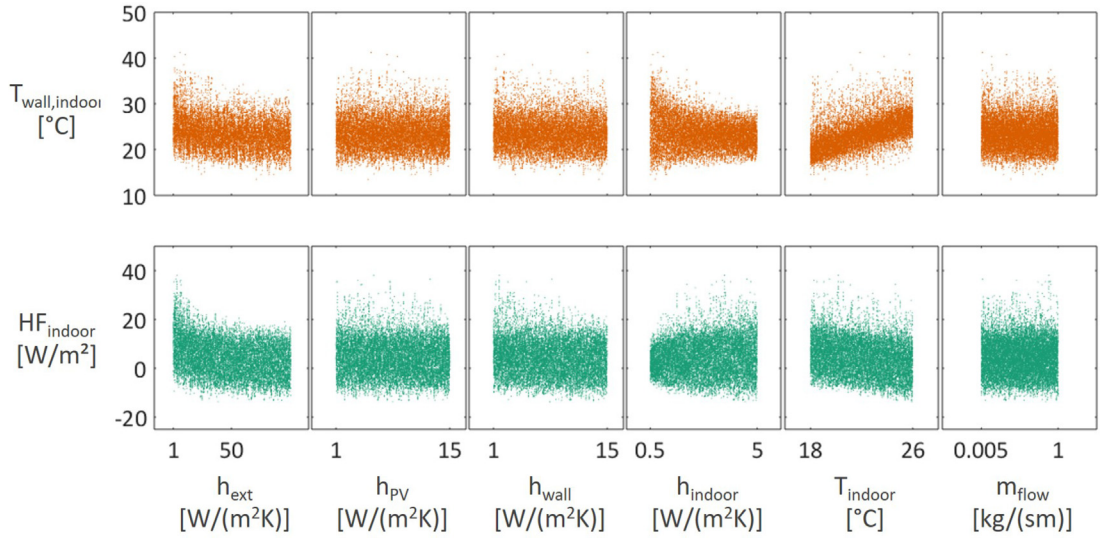

Fig. 14. Scatter plots for a building wall with $R_{wall}/3$ for HF_{indoor} and $T_{wall,\ indoor}$ (Case 1, 20,000 simulations).

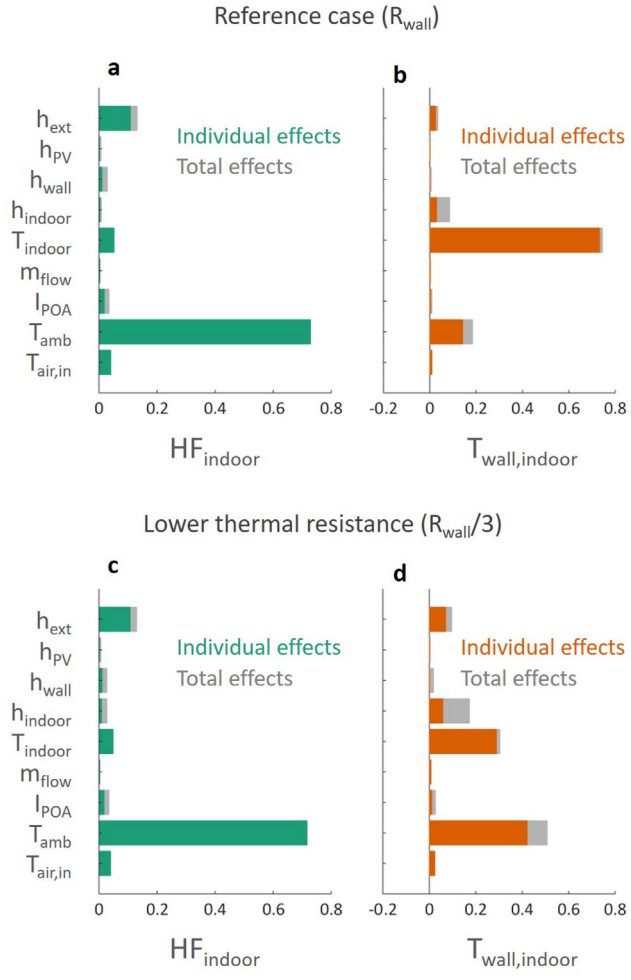

Fig. 15. Sobol indices for HF_{indoor} and $T_{wall,\ indoor}$ (Case 1, 20,000 simulations): a,b) Reference case R_{wall}, and c,d) lower thermal resistance $R_{wall}/3$.

6. Conclusion

This work investigates the behaviour of a naturally ventilated BIPV module for facade applications, using a simulation framework that combines global SA methods with a multi-physics BIPV model developed previously by the authors. The BIPV model has been previously validated using experimental field data. The present work uses this validated BIPV model within a SA framework in order to quantify the influence of several inputs on the BIPV temperature and power predictions (model outputs). The global SA methods ensure that interactions between inputs are considered. In addition, the exterior convective heat transfer coefficient is considered in the analysis as a key input. The consistency of the findings is demonstrated through the application of different SA methods.

The following nine inputs are selected for the SA: (1) the exterior convective heat transfer coefficient, (2) the convective heat transfer coefficient between the PV module and the air inside the cavity, (3) the convective heat transfer coefficient between the building wall and the air inside the cavity, (4) the convective heat transfer coefficient at the building wall interior surface, (5) the indoor temperature, (6) the airflow through inside the cavity, (7) the plane-of-array solar irradiance reaching the BIPV module, (8) the ambient temperature, and (9) the temperature of the air entering the BIPV cavity. In addition to BIPV power and temperature, the following model outputs are evaluated: building wall temperature on both sides and the heat flux into the building interior.

Three cases are defined in this paper to consider the dependence of SA results on the variation range of the inputs. In the first case, all inputs are varied within a broad range, which defines the operating space of naturally ventilated BIPV modules. In the second case, a narrower range is imposed to the solar irradiance, ambient temperature, and air inlet temperature. This case emulates representative operating conditions for BIPV facades, i.e. irradiance around 800 W/m^2 and ambient temperature between 20 and 25 °C. In the third case, the range of the exterior convective heat transfer is reduced significantly. This case represents a situation in which the heat dissipation to the exterior environment is limited.

As expected, the SA results change from one case to the other. In the first case, the relationship between inputs and outputs is distinct for temperature and power. Temperature predictions

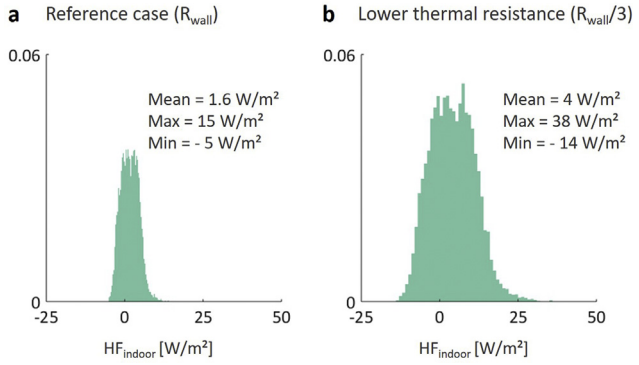

Fig. 16. Influence of the building wall thermal resistance on the heat flux to the indoor environment HF_{indoor}: a) Reference case R_{wall}, and b) lower thermal resistance $R_{wall}/3$.

present some correlation with the exterior convective heat transfer coefficient, the ambient temperature and the temperature of the air entering the BIPV module, while power outputs are mostly affected by the solar irradiance. In the second case, temperature and power seem to respond to the same parameters. In particular, the stronger influence of the exterior convective heat transfer coefficient on both temperature and power is evident. In the third case, the importance of cavity ventilation at less favourable conditions for exterior heat dissipation is highlighted.

Furthermore, a specific trend is observed for the relationship between the exterior convective heat transfer coefficient (h_{ext}) and the BIPV performance. The spread in the predictions decreases as h_{ext} increases (to a rather narrow range at high h_{ext}). This finding has two important implications. First, h_{ext} models should be carefully considered in BIPV modelling, in particular at low h_{ext}, where a small difference in h_{ext} has a relatively large effect on the BIPV performance. Second, a larger spread in the results at low h_{ext} conditions means that the other inputs such as cavity ventilation become relatively more important in these conditions. Therefore, good ventilation conditions should be designed for BIPV modules operating at low h_{ext} conditions (in practice are associated to low wind speeds at the BIPV module). An additional practical implication of the SA results is the distinct behaviour between high and low thermal resistance building walls, corroborating the need for a thermal coupling between BIPV module and the building interior to properly describe the performance of BIPV envelopes.

CRediT authorship contribution statement

Juliana E. Gonçalves: Conceptualization, Methodology, Software, Validation, Formal analysis, Writing - original draft. **Twan van Hooff:** Conceptualization, Writing - review & editing, Supervision. **Dirk Saelens:** Conceptualization, Writing - review & editing, Supervision.

Declaration of competing interest

The authors declare that they have no known competing financial interests or personal relationships that could have appeared to influence the work reported in this paper.

Acknowledgments

Twan van Hooff is currently a postdoctoral fellow of the Research Foundation Flanders (FWO) and acknowledges its financial support (project FWO 12R9718N).

References

[1] Global Alliance for Buildings and Construction, International Energy Agency, and the United Nations Environment Programme, 2019 Global Status Report for Buildings and Construction: towards a Zero-Emission, Efficient and Resilient Buildings and Construction Sector, 2019.
[2] O. Lucon, D. Ürge-Vorsatz, A.Z. Ahmed, H. Akbari, P. Bertoldi, L.F. Cabeza, N. Eyre, A. Gadgil, L. Harvey, Y. Jiang, et al., Buildings., Climate Change 2014: Mitigation of Climate Change. Contribution of Working Group III to the Fifth Assessment Report of the Intergovernmental Panel on Climate Change, Cambridge University Press, Cambridge, United Kingdom and New York, NY, USA, 2014.
[3] IEA, Trends 2018 in Photovoltaic Applications, Tech. Rep, International Energy Agency, 2018.
[4] T. Abergel, B. Dean, J. Dulac, Towards a Zero-Emission, Efficient, and Resilient Buildings and Construction Sector: Global Status Report 2017, Tech. Rep, UN Environment and International Energy Agency, 2017.
[5] D. D'Agostino, L. Mazzarella, What is a nearly zero energy building? Overview, implementation and comparison of definitions, J. Build. Eng. 21 (2018) 200–212.
[6] F.J. Osseweijer, L.B. Van Den Hurk, E.J. Teunissen, W.G. van Sark, A comparative review of building integrated photovoltaics ecosystems in selected European countries, Renew. Sustain. Energy Rev. 90 (2018) 1027–1040.
[7] E. Saretta, P. Caputo, F. Frontini, A review study about energy renovation of building facades with BIPV in urban environment, Sustain. Cities Soc. 44 (2018) 343–355.
[8] S. Aguacil, S. Lufkin, E. Rey, Active surfaces selection method for building-integrated photovoltaics (bipv) in renovation projects based on self-consumption and self-sufficiency, Energy Build. 193 (2019) 15–28.
[9] P. Defaix, W. Van Sark, E. Worrell, E. de Visser, Technical potential for photovoltaics on buildings in the eu-27, Sol. Energy 86 (9) (2012) 2644–2653.
[10] M. Brito, S. Freitas, S. Guimarães, C. Catita, P. Redweik, The importance of facades for the solar PV potential of a Mediterranean city using LiDAR data, Renew. Energy 111 (2017) 85–94.
[11] S. Freitas, M.C. Brito, Solar façades for future cities, Renew. Energy Focus 31 (2019) 73–79.
[12] S. Freitas, M. Brito, Non-cumulative only solar photovoltaics for electricity load-matching, Renew. Sustain. Energy Rev. 109 (2019) 271–283.
[13] R.A. Agathokleous, S.A. Kalogirou, Double skin facades (DSF) and building integrated photovoltaics (BIPV): a review of configurations and heat transfer characteristics, Renew. Energy 89 (2016) 743–756.
[14] T. Yang, A.K. Athienitis, A review of research and developments of building-integrated photovoltaic/thermal (BIPV/t) systems, Renew. Sustain. Energy Rev. 66 (2016) 886–912.
[15] E. Biyik, M. Araz, A. Hepbasli, M. Shahrestani, R. Yao, L. Shao, E. Essah, A.C. Oliveira, T. del Caño, E. Rico, et al., A key review of building integrated photovoltaic (BIPV) systems, Engineering science and technology, Int. J. 20 (3) (2017) 833–858.
[16] R.A. Agathokleous, S.A. Kalogirou, Status, barriers and perspectives of building integrated photovoltaic systems, Energy 191 (2020) 116471.
[17] D. Thevenard, Review and recommendations for improving the modelling of building integrated photovoltaic systems, in: Proceedings of the 9th International IBPSA Conference, Citeseer, Montreal, Canada, 2005.
[18] A. Omazic, G. Oreski, M. Halwachs, G. Eder, C. Hirschl, L. Neumaier, G. Pinter, M. Erceg, Relation between degradation of polymeric components in crystalline silicon pv module and climatic conditions: a literature review, Sol. Energy Mater. Sol. Cell. 192 (2019) 123–133.
[19] M. Halwachs, L. Neumaier, N. Vollert, L. Maul, S. Dimitriadis, Y. Voronko, G. Eder, A. Omazic, W. Mühleisen, C. Hirschl, et al., Statistical evaluation of pv system performance and failure data among different climate zones, Renew. Energy 139 (2019) 1040–1060.
[20] Y.B. Assoa, F. Sauzedde, B. Boillot, Numerical parametric study of the thermal and electrical performance of a bipv/t hybrid collector for drying applications, Renew. Energy 129 (2018) 121–131.
[21] L. Walker, J. Hofer, A. Schlueter, High-resolution, parametric BIPV and electrical systems modeling and design, Appl. Energy 238 (2019) 164–179.
[22] W. Tian, A review of sensitivity analysis methods in building energy analysis, Renew. Sustain. Energy Rev. 20 (2013) 411–419.
[23] Z. Pang, Z. O'Neill, Y. Li, F. Niu, The role of sensitivity analysis in the building performance analysis: a critical review, Energy Build. (2019) 109659.
[24] A. Saltelli, K. Aleksankina, W. Becker, P. Fennell, F. Ferretti, N. Holst, S. Li, Q. Wu, Why so many published sensitivity analyses are false: a systematic review of sensitivity analysis practices, Environ. Model. Software 114 (2019) 29–39.
[25] A. Saltelli, M. Ratto, T. Andres, F. Campolongo, J. Cariboni, D. Gatelli, M. Saisana, S. Tarantola, Global Sensitivity Analysis: the Primer, John Wiley & Sons, 2008.
[26] J. Cipriano, G. Houzeaux, G. Mor, U. Eicker, J. Carbonell, S. Danov, Development of a dynamic model for natural ventilated photovoltaic components and of a data driven approach to validate and identify the model parameters, Sol. Energy 129 (2016) 310–331.
[27] T. Defraeye, B. Blocken, J. Carmeliet, Convective heat transfer coefficients for exterior building surfaces: existing correlations and CFD modelling, Energy Convers. Manag. 52 (1) (2011) 512–522.

[28] M. Mirsadeghi, D. Costola, B. Blocken, J.L. Hensen, Review of external convective heat transfer coefficient models in building energy simulation programs: implementation and uncertainty, Appl. Therm. Eng. 56 (1–2) (2013) 134–151.
[29] H. Montazeri, B. Blocken, New generalized expressions for forced convective heat transfer coefficients at building facades and roofs, Build. Environ. 119 (2017) 153–168.
[30] H. Montazeri, B. Blocken, Extension of generalized forced convective heat transfer coefficient expressions for isolated buildings taking into account oblique wind directions, Build. Environ. 140 (2018) 194–208.
[31] J.D. Herman, W. Usher, Salib: an open-source python library for sensitivity analysis, J. Open Source Soft. 2 (9) (2017) 97.
[32] J.E. Goncalves, T. van Hooff, D. Saelens, A physics-based high-resolution BIPV model for building performance simulations, Sol. Energy 204 (2020) 585–599.
[33] J.E. Goncalves, T. van Hooff, D. Saelens, BIPV Modelling for Building Performance Simulations: Comparison to Experimental Data and Evaluation of Modelling Complexity, 2020. In preparation.
[34] F. Jorissen, G. Reynders, R. Baetens, D. Picard, D. Saelens, L. Helsen, Implementation and verification of the IDEAS building energy simulation library, J. Buil. Perform. Simul. (2018) 1–20.
[35] H. Montazeri, B. Blocken, D. Derome, J. Carmeliet, J.L. Hensen, CFD analysis of forced convective heat transfer coefficients at windward building facades: influence of building geometry, J. Wind Eng. Ind. Aerod. 146 (2015) 102–116.
[36] A. La Pica, G. Rodono, R. Volpes, An experimental investigation on natural convection of air in a vertical channel, Int. J. Heat Mass Tran. 36 (3) (1993) 611–616.
[37] S. Obyn, G. Van Moeseke, Variability and impact of internal surfaces convective heat transfer coefficients in the thermal evaluation of office buildings, Appl. Therm. Eng. 87 (2015) 258–272.
[38] R.A. Agathokleous, S.A. Kalogirou, Part i: thermal analysis of naturally ventilated bipv system: experimental investigation and convective heat transfer coefficients estimation, Sol. Energy 169 (2018) 673–681.
[39] M. Shahrestani, R. Yao, E. Essah, L. Shao, A.C. Oliveira, A. Hepbasli, E. Biyik, T. del Caño, E. Rico, J.L. Lechón, Experimental and numerical studies to assess the energy performance of naturally ventilated pv façade systems, Sol. Energy 147 (2017) 37–51.
[40] D. Saelens, S. Roels, H. Hens, The inlet temperature as a boundary condition for multiple-skin facade modelling, Energy Build. 36 (8) (2004) 825–835.
[41] A. Saltelli, S. Tarantola, K.-S. Chan, A quantitative model-independent method for global sensitivity analysis of model output, Technometrics 41 (1) (1999) 39–56.
[42] M.H. Kristensen, S. Petersen, Choosing the appropriate sensitivity analysis method for building energy model-based investigations, Energy Build. 130 (2016) 166–176.
[43] R. Cukier, C. Fortuin, K.E. Shuler, A. Petschek, J. Schaibly, Study of the sensitivity of coupled reaction systems to uncertainties in rate coefficients. i theory, J. Chem. Phys. 59 (8) (1973) 3873–3878.
[44] I.M. Sobol, Global sensitivity indices for nonlinear mathematical models and their Monte Carlo estimates, Math. Comput. Simulat. 55 (1–3) (2001) 271–280.
[45] A. Saltelli, Making best use of model evaluations to compute sensitivity indices, Comput. Phys. Commun. 145 (2) (2002) 280–297.
[46] A. Saltelli, P. Annoni, I. Azzini, F. Campolongo, M. Ratto, S. Tarantola, Variance based sensitivity analysis of model output. design and estimator for the total sensitivity index, Comput. Phys. Commun. 181 (2) (2010) 259–270.
[47] D. Saelens, S. Roels, H. Hens, The inlet temperature as a boundary condition for multiple-skin facade modelling, Energy Build. 36 (8) (2004) 825–835.
[48] J. Liu, M. Heidarinejad, S. Gracik, J. Srebric, The impact of exterior surface convective heat transfer coefficients on the building energy consumption in urban neighborhoods with different plan area densities, Energy Build. 86 (2015) 449–463.
[49] S. Iousef, H. Montazeri, B. Blocken, P. van Wesemael, Impact of exterior convective heat transfer coefficient models on the energy demand prediction of buildings with different geometry, in: Building Simulation, vol. 12, Springer, 2019, pp. 797–816.
[50] M. T. Kahsay, G. Bitsuamlak, F. Tariku, Effect of localized exterior convective heat transfer on high-rise building energy consumption, in: Building Simulation, Springer, pp. 1–13.
[51] T. Yang, A.K. Athienitis, Experimental investigation of a two-inlet air-based building integrated photovoltaic/thermal (bipv/t) system, Appl. Energy 159 (2015) 70–79.
[52] A. Buonomano, G. De Luca, U. Montanaro, A. Palombo, Innovative technologies for nzebs: an energy and economic analysis tool and a case study of a non-residential building for the mediterranean climate, Energy Build. 121 (2016) 318–343.
[53] A.K. Athienitis, G. Barone, A. Buonomano, A. Palombo, Assessing active and passive effects of façade building integrated photovoltaics/thermal systems: dynamic modelling and simulation, Appl. Energy 209 (2018) 355–382.